

Received: 2019.04.06

Accepted: 2019.06.28

Published: 2019.07.15

Imaging Analysis of Ganglioneuroma and Quantitative Analysis of Paraspinal Ganglioneuroma

Authors' Contribution:

Study Design A
Data Collection B
Statistical Analysis C
Data Interpretation D
Manuscript Preparation E
Literature Search F
Funds Collection G

ABCDE 1 **Li Luo***
CDEF 1 **Xue Zheng***
BC 2 **Kai-Zhong Tao***
ABCD 3 **Jiang Zhang***
DEF 4 **Yue-Yang Tang**
ADEF 1 **Fu-Gang Han**

1 Department of Radiology, The Affiliated Hospital of Southwest Medical University, Luzhou, Sichuan, P.R. China
2 Department of Neurosurgery, The People's Hospital of Zhongjiang, Deyang, Sichuan, P.R. China
3 Department of Thoracic Surgery, The People's Hospital of Zhongjiang, Deyang, Sichuan, P.R. China
4 Department of Pathology, The Affiliated Hospital of Southwest Medical University, Luzhou, Sichuan, P.R. China

* Li Luo, Xue Zheng, Kai-Zhong Tao, and Jiang Zhang contributed equally to this study

Corresponding Author: Fu-Gang Han, e-mail: kaiztao@foxmail.com

Source of support: Departmental sources

Background: This study evaluated the imaging features of ganglioneuroma (GN) and assessed the diagnostic value of the enhancement rate (ER) of CT for GN.

Material/Methods: We retrospectively reviewed records of 49 patients with histopathologically confirmed GN who underwent preoperative contrast-enhanced CT or MRI between 2010 and 2018. The independent samples *t* test and chi-square test were used. Receiver operating characteristic (ROC) curves were generated to analyze the diagnostic sensitivity (SE) and specificity (SP). Positive predictive value (PPV) and negative predictive value (NPV) were calculated.

Results: The CT values were 32.59 ± 3.61 Hounsfield units (HU) for plain scans, 38.87 ± 5.09 HU for the arterial phase, and 54.26 ± 8.14 HU for the venous phase, and the incidence of calcification and cysts was 32.6% and 10.2%, respectively. There was no significant difference in CT results and clinical parameters between mediastinal ganglioneuroma (MGN) and retroperitoneal ganglioneuroma (RGN) ($p > 0.05$). The area under the curves (AUCs) for the arterial enhancement rate (AER), venous enhancement rate (VER), and AER/VER combined index in diagnosing GN were 0.735, 0.980, and 0.990, respectively. The VER of 0.2819 exhibited the SE and SP at 92.9% and 92.9%, respectively, to characterize the GN, whereas the AER of 0.1779 had SE and SP of 52.4% and 90.5%, respectively. The SE and SP for the combined index were 88.1% and 100%, respectively. The GN showed hypointensity on T1WI, hyperintense, or slightly high signal on T2WI with the linear hypointensity, and hyperintense on DWI.

Conclusions: A hypodense mass was observed for GN on plain scan and presented delayed enhancement on contrast enhancement. VER or AER/VER combination is more accurate than AER for the diagnosis of paravertebral GN.

MeSH Keywords: **Ganglioneuroma • Magnetic Resonance Imaging • Tomography, Spiral Computed**

Full-text PDF: <https://www.medscimonit.com/abstract/index/idArt/916792>

 2985

 4

 5

 29



Background

Ganglioneuroma (GN) is a rare type of benign tumor, estimated to account for 0.1% to 0.5% of all central nervous system tumors [1]. GN are believed to originate from primitive neural crest cells, and they are mainly distributed in the mediastinum (41.5%), retroperitoneum (37.5%), and neck (8%) [1–4]. There are also some case reports describing GN in the spinal canal, trigeminal nerve, and jugular foramen [5–8]. GN most often manifest as an asymptomatic mass and are found incidentally [3,9,10]. It has also been reported that adrenal GN can secrete dopamine, vasoactive intestinal peptide, and cortisol, leading to hypertensive crisis, diarrhea, and male-like metabolic disorders in women [11–14].

GN behave aggressively, and recurrence or malignant transformation has been reported, although they are histologically benign [3,15,16]. Due to these characteristics, surgical resection is the first and the optimal choice for complete cure [14,17]. GN usually presents as a hypodense mass that is often confused with a cystic lesion. Various surgical procedures are performed to treat benign cystic tumors that are detected before physical surgery, and to treat ganglioneuroma, which is a solid tumor [18]. Therefore, reliable and accurate diagnosis before surgery improves disease management.

Most recent reports on GN describe the imaging features of tumors that have occurred in single locations, with a lack of quantitative analysis. In this study, we analyzed the imaging features of GN and assessed the diagnostic value of the ER of computed tomography (CT) in GN.

Material and Methods

Ethics approval for this retrospective study was obtained from the Institutional Review Board of the Affiliated Hospital of Southwest Medical University. This study evaluated patients who were examined and treated at the institution between January 1, 2010, and July 31, 2018.

Patients inclusion

This study retrospectively reviewed records of patients with pathologically proven GN who underwent contrast-enhanced CT or magnetic resonance imaging (MRI) before surgery, and then underwent curative surgery for GN. All of the data were available in the picture archiving and communication system (PACS). The exclusion criteria were: undergoing only ultrasound before surgery and absence of a presurgical CT or MRI scan in the local PACS; undergoing CT without intravenous contrast administration; not undergoing surgical resection of tumors or undergoing surgery performed at other institutions;

having multiple tumors and a pathology report that was not clear about the location of the GN; and no relevant imaging examination was performed at the follow-up after surgery.

CT and MRI technique

There were 44 (89.7%) lesions that were identified from contrast-enhanced CT studies, and 7 (14.3%) lesions were identified from contrast-enhanced MRI studies, with 2 of them having both CT and MRI data. A total of 80–120 ml of nonionic iodinated contrast material (370 mg I/mL) was injected IV at 2.5–3.0 mL/s in all patients who underwent CT scans. CT scans of the neck (n=2) were obtained with a slice thickness of 3 mm and table feed of 15 mm/s at 120 kV and 280 mA. Scanning of the chest (n=23) was performed with a slice thickness of 5 mm, table feed of 15 mm/s, and tube voltage of 120 kV. CT scans of the abdomen (n=19) were obtained with a slice thickness of 5 mm, table feed of 15 mm/s, and tube voltage of 120 kV.

MRI was performed using a Achieva 1.5T magnet (Philips Medical system, Best, the Netherlands) with a torso or spine phased-array coil using the following sequences: axial T1-weighted fast spin-echo (FSE), axial, coronal, and sagittal T2-weighted FSE, axial and coronal T2-weighted spectrally selective attenuated inversion recovery (SPAIR), axial diffusion-weighted imaging sequence (b=800 ms), and T1-weighted gadolinium-enhanced FSE. Gadolinium diethylenetriaminepentaacetic acid (Gd-DTPA) was administered at a dose of 0.1 mmol/kg, and gadolinium-enhanced imaging was performed after unenhanced acquisitions.

CT and MRI qualitative image analysis

Two radiologists (with 10 and 12 years of experience in the interpretation of CT and MRI images) reviewed the images with the routine clinical PACS software used by all physicians at our institution. The images were independently assessed, and the readers were blinded to the operation records, pathologic results, and information provided by other imaging studies, such as ¹⁸F-fluorodeoxyglucose (18F-FDG) PET/CT or ultrasound. The CT and MRI features evaluated were tumor location, site and morphology, presence of calcification, cysts and fat, presence of heterogeneous enhancement, vascular involvement, and lymphadenopathy. In addition, the signal characteristics of the lesions on each sequence were evaluated if the patient underwent MRI.

Tumor locations included the mediastinum, retroperitoneum (including adrenal glands), intraspinal canal, and neck, and the tumor site was recorded as left or right. The morphology of the tumor was described as regular or irregular, with a round or oval shape classified as regular and a lobular shape or dumb-bell shape classified as irregular.

On CT or MRI contrast-enhanced images, lesions were defined as heterogeneous if cystic components were confirmed within the lesions, or the lesions appeared as flocculent or with patchy enhancement. Vascular involvement was considered present if the tumor enclosing or adjacent to the vessel was accompanied by narrowing or a distortion or filling defect. Lymphadenopathy was reported when peritumoral lymph nodes were larger than 1.0 cm with irregular margins and heterogeneous enhancement.

CT quantitative image analysis

Only 42 cases of paraspinal GN (retroperitoneal GN and mediastinal GN) were evaluated for our quantitative study because the 2 GNs occurring in the neck and spinal canal were too small for statistical analysis. The PACS workstation was used by 2 readers to independently obtain measurements. The 2 readers measured the longest diameter of the GN and calculated the average.

The freehand region of interest (ROI) drawing tools were used to measure the CT value of the GN, which included 1/2 to 3/4 areas of the solid portion of the mass, and this generated the minimum, maximum, and mean of the lesion's CT attenuation in Hounsfield units. When outlining the ROI, the center of the lesion was measured to avoid calcification, fat, and cysts and to prevent the partial volume effect. We selected the enhanced area as the ROI when the tumor showed inhomogeneous enhancement on a contrast-enhanced scan to better assess the enhancement degree and ER, and we outlined the corresponding regions on non-contrast CT images. We measured the CT density of the erector spinal muscles, which was on the same layer and side with lesions, and tried to avoid the intermuscular space. We ensured that the ROI sites and areas were the same in the same patient during the 3 phases. Measurements were repeated 3 times at different layers in each period, and the average was calculated.

We classified the degree of CT enhancement [19] as no enhancement (<10 HU), slight (10–20 HU), moderate (20–50 HU), or marked (>50 HU), while the degree of MRI enhancement was classified as no enhancement, mild (lower than that of muscle tissue), moderate (equal to that of muscle tissue), or marked (higher than that of muscle tissue). The ER of CT was calculated in each phase for the erector spinal muscles and GN, respectively. Arterial enhancement ratio (AER)=(arterial-unenhanced)/unenhanced, and venous enhancement ratio (VER)=(venous-unenhanced)/unenhanced, in which unenhanced, arterial, and venous are the mean attenuations for the unenhanced (plain scan), arterial, and venous phases, respectively, on contrast-enhanced CT.

Clinical, surgical, and pathological analysis

We searched the medical record system software that collected clinical data for patients who met our inclusion criteria.

Clinical data included age, sex, and medical history (chief complaint, hypertension, diabetes mellitus, and coronary heart disease). We also focused on whether hormonal abnormalities were present by examining the hormone levels for each patient. We recorded the intraoperative discovery in the medical records system to accurately characterize the GN location and texture, the relationship between tumors and adjacent tissues, and to determine whether there was vascular involvement. Pathological patient images were collected in the pathological inquiry system, and their components were analyzed by an experienced pathologist.

Follow-up assessment

We evaluated the postoperative CT or MRI images of our patients to assess their outcomes. Two readers recorded whether the patient developed local recurrence and whether the patient developed regional or distant metastatic disease. The time interval between surgery and the postoperative CT or MRI was recorded.

Receiver operating characteristic (ROC) curve analysis

The diagnostic value of AER, VER, and AER/VER combined index in terms of GN were determined by performing ROC curve analysis, using GraphPad Prism (version 8.1). The AER, VER, and AER/VER combined index for the erector spinal muscles were calculated and used as the negative control. The AER/VER combined index was calculated by the following formula: $B1 \times AER + B2 \times VER$. B1 and B2 refers to the coefficient of AER and VER in the linear regression model by setting GN as the dependent variable, using the enter method in SPSS. The value of the area under the curve (AUC) of each curve was calculated and compared. The threshold was evaluated, and the sensitivity (SE), specificity (SP), negative predictive value (NPV), and positive predictive value (PPV) of each measure were computed from a generalized estimating equation. The DeLong test was conducted to compare ROC curves.

Statistical analysis

Data analysis was performed using SPSS software (version 22.0) and GraphPad Prism (version 8.1). Two-tailed $p < 0.05$ was considered significant. Continuous data are reported as the mean \pm standard deviation (SD), and were compared by independent samples t test after homogeneity of variance if they conformed to normal distribution. The continuous variable of non-normal distribution is represented by the median. Normal transformation was carried out if the quantitative data did not conform to normal distribution, and then, the independent samples t test was used for comparison. The Mann-Whitney-Wilcoxon test was used when the continuous variable did not conform to normal distribution after normal transformation.

Table 1. Clinical and demographic characteristics of GN included in this study (n=49).

Characteristics	Value
Mean age in years at diagnosis (range)	32.9 (4–62) years
Sex	
Female (%)	47%
Male (%)	53%
Clinical presentations	
Incidental	29 (59.2%)
Abdominal/back/chest discomfort	9 (18.4%)
Limb numbness/painfulness	8 (16.3%)
Postauricular swelling and tenderness	1 (2%)
Shortness of breath after exercise	1 (2%)
Phlegm with blood	1 (2%)

Characteristics	Value
Tumor site	
Right	34 (69.3%)
Left	15 (30.7%)
Tumor location	
Mediastinum	23 (46.9%)
Retroperitoneum (including 17 adrenal gland cases)	19 (38.8%)
Intraspinal canal	5 (10.2%)
Neck	2 (4.1%)
Mean preoperative tumor size in cm (range)	1.7–10.2
Mean tumor size in cm on pathology in cm (range)	2.1–12.0

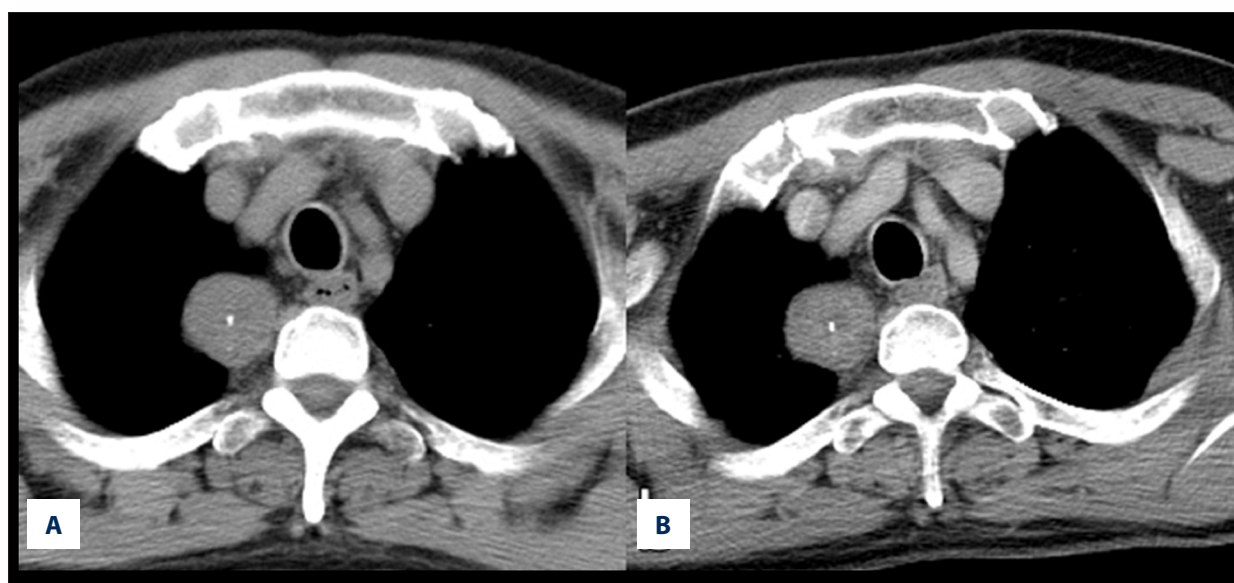


Figure 1. GN of the right mediastinum. A 50-year-old man with ganglioneuroma of the right anterior mediastinum. (A) Plain scan demonstrates punctate calcification in the center of a hypodensity mass. (B) The mass showed mild enhancement in venous phase.

The chi-square test was used for comparison between categorical variables, which are presented as percentages.

Results

Patient demographics and clinical characteristics

Patient demographics and clinical characteristics are summarized in Table 1. None of the patients in our study exhibited any

hormonal abnormalities. The longest follow-up time was approximately 2 years, the shortest was approximately 6 months, and none of the patients developed local recurrence or regional or distant metastases.

CT and MRI features

All of the lesions of our study were unilateral, and 34 cases (69.3%) were located on the right side of the spine. The CT value of plain scans (32.59 ± 3.61 HU) in 42 cases was lower than

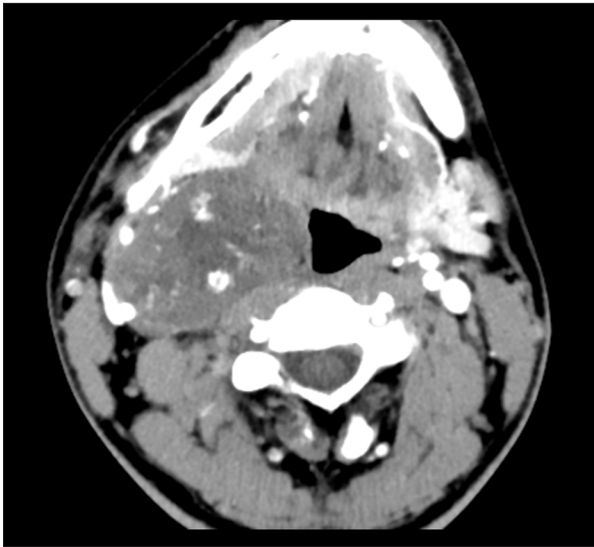


Figure 2. GNs in the right neck. A 22-year-old man with ganglioneuroma in the medial sheath of the right carotid artery, with unenhanced cystic area and enclosed vessels.

the muscle density (53.78 ± 4.51 HU) at the same section. The CT values of the arterial and venous phase were 38.87 ± 5.09 HU and 54.26 ± 8.14 HU, respectively. The MRI for 7 patients showed hypointensity on T1-weighted image (T1WI) ($n=7$), hyperintense ($n=4$) or slight high signal ($n=3$) on T2-weighted image (T2WI), and hyperintense on diffusion-weighted imaging (DWI) ($n=7$) and SPAIR. Linear hypointensity could be seen in lesions with hyperintensity on T2WI ($n=3$). All of the patients with MRI contrast enhancement showed mild ($n=5$) or moderate ($n=2$) enhancement. The density or signal was homogeneous in 30 cases (61.2%) and heterogeneous in 19 cases (38.7%) on plain scan (including CT and MRI). There were 16 cases (32.6%) that

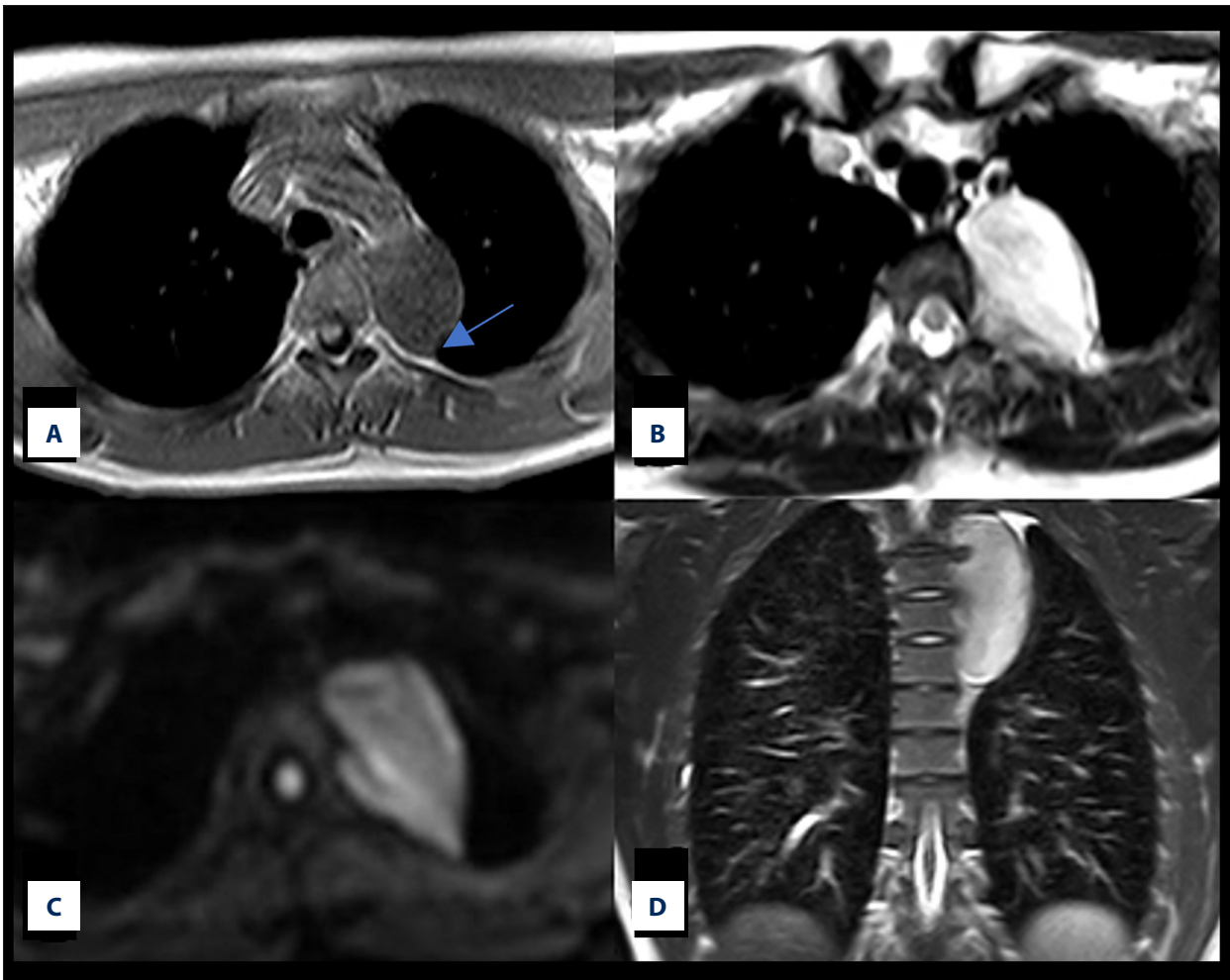


Figure 3. MRI images of GN. A 16-year-old girl with ganglioneuroma in the left mediastinum. (A) A tail-like (blue arrow) was noted on T1WI. (B) A linear hypointense area was noted, which is called “stipe sign”, on T2WI. (C) Diffusion of tumors on DWI was limited and showed high signal intensity. (D) The GN showed signs of a pseudopod that grew in the adjacent intervertebral space in the coronal view with a longitudinal diameter greater than the transverse diameter.

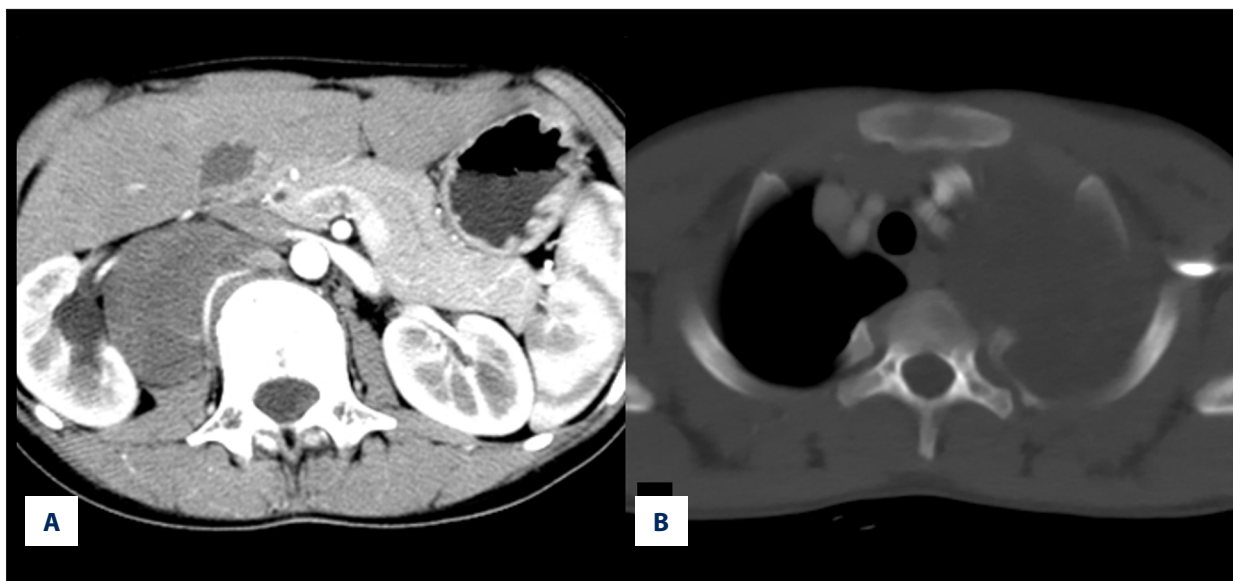


Figure 4. CT findings of GN in different parts. (A) A 12-year-old boy with ganglioneuroma in the right adrenal gland, with the right lumbar artery passing through the lesion, but no invasion, and the compression of ipsilateral ureter leads to hydronephrosis. (B) A 12-year-old boy with ganglioneuroma in the left mediastinum, showing bone resorption in the left rib.

Table 2. Comparison of the CT results of GN in different locations.

Location	Age	CT value			ER	
		NE	A	V	A	V
RGN	32.16±15.52	33.10±3.36	40.12±5.71	52.78±7.8	-0.72±0.20	0.72±0.23
MGN	33.35±15.41	32.18±3.90	37.83±4.38	57.74±9.73	-0.82±0.26	0.65±0.25
<i>t</i> Value	-0.457	0.806	1.466	1.831	1.320	0.916
<i>p</i> Value	0.650	0.425	0.150	0.075	0.194	0.365

NE – non-enhancement; A – arterial phase; V – venous phase.

Table 3. Comparison of the clinical parameters of GN in different locations.

Location	Sex		Site		Longest diameter		Calcification	
	F	M	R	L	≥5 cm	<5 cm	Yes	No
RGN	10	9	15	4	8	11	5	14
MGN	10	13	13	10	13	10	8	15
Chi-square value	0.349		2.335		0.865		0.349	
<i>p</i> Value (2-tailed)	0.554		0.125		0.352		0.555	

presented calcification in our study (Figure 1), and 5 cases (10.2%) presented cysts, with 2 cases showing concurrent calcification and cystic degeneration (Figure 2).

There were 14 cases (28.6%) with irregular morphology in the form of lobulated (n=4), dumbbell (n=3), or pseudopod signs on coronal and sagittal views (n=7), and a tail-like extension was seen in 6 cases of mediastinal ganglioneuroma (MGN) (Figure 3A–3D).

Adjacent tissues were pushed or compressed in 31 cases (63.3%), including 2 cases of GN located in the adrenal gland that resulted in ipsilateral hydronephrosis (Figure 4A). Blood vessels went through or were embedded in the tumor in 7 cases (14.2%), but the lumen was not narrowed, nor was there a filling defect. Local bone resorption and destruction was observed in 2 cases (3.9%) due to the compression of local bone (Figure 4B). Areas with fat and lymphadenopathy were not found in any of our cases.

Table 4. AUC for AER, VER, and AER/VER combined index in diagnosing GN.

Parameter	AER	VER	AER/VER combined index
AUC	0.735	0.98	0.99
95% CI	0.627 to 0.825	0.923 to 0.998	0.938 to 1.000
Significance level	$p < 0.001$	$p < 0.001$	$p < 0.001$
SP	90.50%	92.90%	100.00%
SE	52.40%	92.90%	88.10%
PPV	82.10%	93.00%	100.00%
NPV	65.00%	91.10%	87.50%

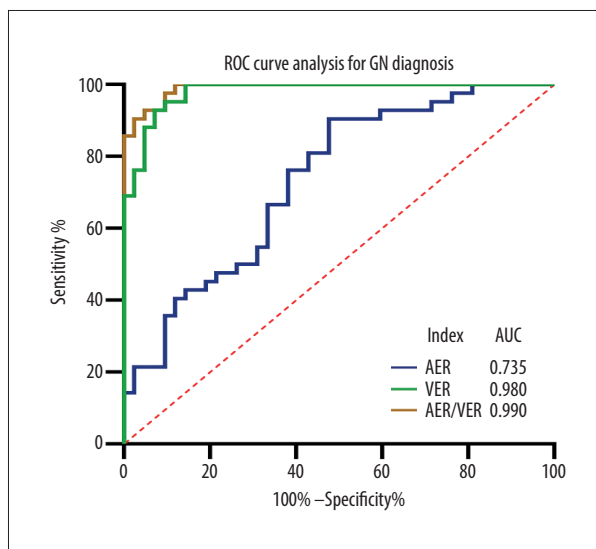


Figure 5. ROC curves showing the diagnostic value of AER, VER, and AER/VER combined index in terms of GN.

Comparison of the CT results and clinical parameters between MGN and RGN

Tables 2 and 3 show the comparison of the CT results and clinical parameters of MGN and retroperitoneal ganglioneuroma (RGN), respectively. Statistical analysis showed no significant difference for each variable, whether the tumor occurred to the mediastinum or retroperitoneum ($P > 0.05$), and regardless of the imaging findings (Table 2) or clinical features (Table 3). This was the premise of the unified analysis of paravertebral GN with ROC curves.

ROC curve analysis of the diagnostic value of AER, VER, and AER/VER combined index in terms of GN

Table 4 and Figure 5 illustrate the ROC curve analysis of AER, VER, and AER/VER combined index in diagnosing GN. To generate a SystemAER/VER combined index, we constructed a linear regression model that included both AER and VER

as independent variables and GN as the dependent variable. In this model, the coefficient for AER was -0.963 and 1.638 for VER. Therefore, the AER/VER combined index was calculated with the formula: $-0.963 \times \text{AER} + 1.638 \times \text{VER}$. ROC curve analysis showed that the AUCs for AER, VER, and AER/VER combined index for GN diagnosis were 0.735 , 0.980 , and 0.990 , respectively (Figure 5).

Discussion

GN has heterogenous compositions, which include Schwann cells, mature ganglion cells, nerve fibers, and mucus matrix [20,21]. The mucus matrix is rich in hydrophilic acidic mucopolysaccharide, which constantly absorbs water; therefore, GN appeared as a hypodense mass on the pre-contrast CT scan. With an increase in cells and a decrease in the mucous matrix, the density of lesions may be slightly increased, but the CT value of GN on plain scan is always lower than that of muscle on the same layer. The myxoid matrix components of GN delay the absorption of contrast media, which leads to delayed enhancement [18,22].

We found that the diagnostic efficiency of the AER (AUC=73.5%) was lower than that of the VER (AUC=98.0%), and the difference in the AUC was statistically significant ($p < 0.001$). The combined index of AER/VER showed an AUC of 0.99 , which was superior to the AUC of the AER ($p < 0.001$), but there was no significant difference in comparison to that of the VER ($p = 0.21$). The combination of ERs yielded the highest SP and PPV (both 100%), while VER had the highest SE (92.9%) and NPV (91.1%). The SE (52.4%), SP (90.5%), PPV (82.1%), and NPV (65%) of the AER were the lowest, which indicates that the AER is not a reliable indicator for diagnosing paravertebral GN compared with the other 2 indicators.

GN showed hypointensity on T1WI, heterogeneous hyperintensity on T2WI, and hyperintensity on SPAIR. Previous studies suggested that a whorled pattern (a low-signal part is found

in T2WI when the mass is shown in a high signal) is the characteristic appearance of GN, and it corresponds to the microscopic interlacing patterns of Schwann cells and collagen fibers [23,24]. Of the 7 patients who underwent MRI, 3 exhibited linear hypointensity on T2WI and we called it the "stripe sign", which shares similarities with the whorled pattern. However, we have insufficient MRI images for the optimal analysis of GN, and big-data research is required to confirm this finding. We also found that all GN exhibited hyperintensity predominant on DWI, which is consistent with the mucus matrix of GN, and this effect helps differentiate GN from cysts. Therefore, we speculate that this phenomenon is a characteristic sign of GN diagnosis and increased attention to DWI and ADC values might improve our understanding of GN in the future.

Punctate or discrete calcifications have been previously noted in 20–60% of GN [25,26], and there were 16 cases (32.6%) in our study that were consistent with those reports. Duffy et al. [27] considered that fat replacement might be characteristic of GN. However, of the 49 cases, no fat component was found, and we speculate that there is an extremely low incidence of this sign. Additionally, a few of the relevant studies were case reports [20,27]. For some patients (n=6) in our study, some of the MGN exhibited a tail-like extension, which was consistent with the report of Maho Kato et al. [28]. We considered that the appearance of this sign was caused by the extension of the GN to the nerve branches, or the pushing of adjacent pleura by the GN. GN present the pseudopodia sign when they grow to the interspace between adjacent tissues, and this is considered to be another characteristic of GN, which was observed in 8 cases (16.3%).

Both this study and previous reports indicated a similar GN morbidity between males and females [4,14,29]. However, it seems strange that GN tends to occur on the right side of the spine, and this requires further study. It is a remarkable fact that the blood vessels are only pushed and displaced, not

narrowed or invaded, although the tumor often surrounds or compresses them [18]. This finding further suggests that GN are benign tumors.

This study has a few limitations. Firstly, only a few patients underwent MRI scans, and there were no multiphase contrast-enhanced MRI scans performed, which limits the comprehensiveness of MR imaging. Secondly, because of the low incidence of cervical and spinal canal GN, only quantitative analysis of paraspinal GN may not provide a complete range of CT enhancement rates for GN.

Conclusions

In summary, GN appears as hypodense masses on plain scan and presents delayed enhancement on contrast enhancement. With a threshold of VER >0.2819 , the SE and SP were 92.9% and 92.9%, respectively, for characterizing paravertebral GN. The combination of AER and VER had high SP in the diagnosis of paravertebral GN, but the SE was lower than that of VER in the venous phase. Thus, it is not recommended to use AER alone as an indicator for diagnosing paravertebral GN. The T2WI with stripe sign may be helpful in the diagnosis of GN, and hyperintense signal on DWI may be one of the characteristic signs helpful in the diagnosis of GN, but this needs further research.

Acknowledgments

We thank LetPub for its linguistic assistance during the preparation of our manuscript.

Conflicts of interest

None.

References:

- Shimada H, Ambros IM, Dehner LP et al: Terminology and morphologic criteria of neuroblastic tumors: Recommendations by the International Neuroblastoma Pathology Committee. *Cancer*, 1999; 86: 349–63
- Johnson GL, Hruban RH, Marshall FF, Fishman EK: Primary adrenal ganglioneuroma: CT findings in four patients. *Am J Roentgenol*, 1997; 169: 169–71
- Loneragan GJ, Schwab CM, Suarez ES, Carlson CL: Neuroblastoma, ganglioneuroblastoma, and ganglioneuroma: Radiologic-pathologic correlation. *Radiographics*, 2002; 22: 911–34
- Geoerger B, Hero B, Harms D et al: Metabolic activity and clinical features of primary ganglioneuromas. *Cancer*, 2001; 91: 1905–13
- Wang JT, Wang AY, Cheng S et al: Jugular foramen ganglioneuroma presenting radiographically as Schwannoma. *Otol Neurotol*, 2016; 37: e319–21
- Yilmaz B, Toktas ZO, Akakin A et al: Lumbar spinal immature ganglioneuroma with conus medullaris invasion: Case report. *Pediatr Neurosurg*, 2015; 50: 330–35
- Deng X, Fang J, Luo Q et al: Advanced MRI manifestations of trigeminal ganglioneuroma: A case report and literature review. *BMC Cancer*, 2016; 16: 694
- Ulusoy OL, Aribal S, Mutlu A et al: Ganglioneuroma of the lumbar spine presenting with scoliosis in a 7-year-old child. *Spine J*, 2016; 16: e727
- Yam B, Walczyk K, Mohanty SK et al: Radiology-pathology conference: Incidental posterior mediastinal ganglioneuroma. *Clin Imaging*, 2009; 33: 390–94
- Decarolis B, Simon T, Krug B et al: Treatment and outcome of ganglioneuroma and ganglioneuroblastoma intermixed. *BMC Cancer*, 2016; 16: 542
- Erem C, Kocak M, Cinel A, Erso HO, Reis A: Dopamine-secreting adrenal ganglioneuroma presenting with paroxysmal hypertension attacks. *Saudi Med J*. 2008;29: 122-125.
- Koch CA, Brouwers FM, Rosenblatt K et al: Adrenal ganglioneuroma in a patient presenting with severe hypertension and diarrhea. *Endocr Relat Cancer*, 2003; 10: 99–107

13. Diab DL, Faiman C, Siperstein AE et al: Virilizing adrenal ganglioneuroma in a woman with subclinical Cushing syndrome. *Endocr Pract*, 2008; 14: 584–87
14. Barrena Lopez C, De la Calle Garcia B, Sarabia Herrero R: Intradural ganglioneuroma mimicking lumbar disc herniation: Case report. *World Neurosurg*, 2018; 117: 40–45
15. Hayashi Y, Iwato M, Hasegawa M et al: Malignant transformation of a gangliocytoma/ganglioglioma into a glioblastoma multiforme: A molecular genetic analysis. Case report. *J Neurosurg*, 2001; 95: 138–42
16. Kulkarni AV, Bilbao JM, Cusimano MD, Muller PJ: Malignant transformation of ganglioneuroma into spinal neuroblastoma in an adult. Case report. *J Neurosurg*, 1998; 88: 324–27
17. Fraga JC, Aydogdu B, Aufieri R et al: Surgical treatment for pediatric mediastinal neurogenic tumors. *Ann Thorac Surg*, 2010; 90: 413–18
18. Guan YB, Zhang WD, Zeng QS et al: CT and MRI findings of thoracic ganglioneuroma. *Br J Radiol*, 2012; 85: e365–72
19. Liu Z, Lv X, Wang W et al: Imaging characteristics of primary intracranial teratoma. *Acta Radiol*, 2014; 55: 874–81
20. Ko SM, Keum DY, Kang YN: Posterior mediastinal dumbbell ganglioneuroma with fatty replacement. *Br J Radiol*, 2007; 80: e238–40
21. Herr K, Muglia VF, Koff WJ, Westphalen AC: Imaging of the adrenal gland lesions. *Radiol Bras*, 2014; 47: 228–39
22. Otal P, Mezghani S, Hassissene S et al: Imaging of retroperitoneal ganglioneuroma. *Eur Radiol*, 2001; 11: 940–45
23. Zhang Y, Nishimura H, Kato S et al: MRI of ganglioneuroma: Histologic correlation study. *J Comput Assist Tomogr*, 2001; 25: 617–23
24. Forsythe A, Volpe J, Muller R: Posterior mediastinal ganglioneuroma. *Radiographics*, 2004; 24: 594–97
25. Wang F, Liu J, Zhang R et al: CT and MRI of adrenal gland pathologies. *Quant Imaging Med Surg*, 2018; 8: 853–75
26. Ichikawa T, Ohtomo K, Araki T et al: Ganglioneuroma: Computed tomography and magnetic resonance features. *Br J Radiol*, 1996; 69: 114–21
27. Duffy S, Jhaveri M, Scudierre J et al: MR imaging of a posterior mediastinal ganglioneuroma: Fat as a useful diagnostic sign. *Am J Neuroradiol*, 2005; 26: 2658–62
28. Kato M, Hara M, Ozawa Y et al: Computed tomography and magnetic resonance imaging features of posterior mediastinal ganglioneuroma. *J Thorac Imaging*, 2012; 27: 100–6
29. Mounasamy V, Thacker MM, Humble S et al: Ganglioneuromas of the sacrum – a report of two cases with radiologic-pathologic correlation. *Skeletal Radiol*, 2006; 35: 117–21